Journal of Advances and Scholarly Researches in Allied Education
Vol. 19, Issue No. 3, April-2022, ISSN 2230-7540

A Study of Photocatalytic Activity Towards the Degradation of Organic Pollutants Under Visible Light Irradiation

Km. Manisha Verma[1]*, Dr. Anil Sharma[2]

[1] PhD Student, Kalinga University Raipur CG

[2] PhD Guide, Kalinga University Raipur CG.

Abstract - This study investigates the photocatalytic activity of a specific material in the degradation of organic pollutants under visible light irradiation. The growing concern over environmental pollution caused by organic pollutants necessitates the development of efficient and sustainable degradation methods. Photocatalysis, which utilizes semiconducting materials to harness solar energy and degrade pollutants, has emerged as a promising solution. However, most studies focus on photocatalytic activity under ultraviolet (UV) light, limiting its practical application. In this research, we explore the visible light photocatalytic activity of a novel material and evaluate its performance in degrading organic pollutants. The material's synthesis, characterization, and photocatalytic experiments were conducted, and the degradation efficiency of various organic pollutants was measured. The results demonstrate the material's significant visible light photocatalytic activity and its potential as an effective tool for organic pollutant degradation under solar light.

Keyword - Photocatalysis, Visible light,

----------X----------

INTRODUCTION

Nanocomposites are composite materials made up of two or more nanoscale materials, each with its own unique physical, chemical, and mechanical characteristics. In recent years, nano-composites' potential uses in photocatalysis—the use of light energy to kickstart chemical reactions—have been the subject of intense research. Due to its great efficiency and lack of environmental impact, photocatalysis has been extensively employed for the elimination of organic contaminants in water and air. When synthesizing nanocomposites for photocatalysis, one material is combined with another that can boost its photocatalytic properties. Among them is graphene oxide (GO), which excels at electron transport despite its small size and enormous surface area. Nanocomposites of GO and photocatalytic materials like titanium dioxide (TiO2) are simple to create by functionalization. TiO2/GO nanocomposites are synthesized using the hydrothermal approach, which requires the application of both heat and pressure during the synthesis process. Methods including X-ray diffraction (XRD), transmission electron microscopy (TEM), Fourier transform infrared spectroscopy (FTIR), and ultraviolet-visible spectroscopy (UV-vis) are then used to describe the nanocomposites and verify their structure, morphology, and optical characteristics. Degradation of organic contaminants in the presence of visible light is used to assess the photocatalytic efficacy of TiO2/GO nanocomposites. The findings demonstrate that the synergistic impact of GO and TiO2 leads in greater photocatalytic activity in the TiO2/GO nanocomposites compared to pure TiO2. Water and air purification are only two potential uses since the nanocomposites are so durable and versatile. [8]

For the photocatalytic destruction of organic pollutants using visible light, nanocomposites have emerged as a potential material. Two or more of these components work together to improve the material's overall performance. Titanium dioxide (TiO2) and carbon-based materials like graphene or carbon nanotubes are one example of such a nanocomposite. By absorbing visible light and transmitting that energy to TiO2, the carbon-based substance functions as a sensitizer, causing the latter to produce reactive oxygen species that may degrade organic pollutants. Nanocomposites of silver and zinc oxide (ZnO) provide still another example. By absorbing visible light and producing localized surface plasmon resonance (LSPR), silver functions as a plasmonic material that boosts the photocatalytic activity of zinc oxide. This is because the LSPR is strongly coupled to the ZnO semiconductor, resulting in enhanced electron-hole separation and greater efficiency.[9]

LITERATURE REVIEW

Zhou et al. [1] Using zinc nitrate hexahydrate and grapheme oxide as raw materials, a ZnO-Reduced graphene hybrid was synthesized using a hydrothermal technique at a pH=11 condition. The shape of ZnO nanostructures such nanoparticles and nanorods was drastically affected by the different mass ratios of zinc nitrate hexahydrate to GO employed to create ZnO-RGO. When exposed to UV light, ZnO-RGO photocatalytically degrades Methylene Blue at a high rate..

Huo et al. [2] revealed a scalable method for making microspheres of ZnO/ZnAl2O4 from the ZnAl-LDH precursor. The ZnO/ZnAl2O4 microspheres have much better photodegradation capability to methylene blue (MB) than the commercial ZnO powder, as shown by photocatalytic assessment under UV irradiation..

Yi et al. [3] nanoflowers of ZnO and Fe/ZnO were produced using a straightforward hydrothermal method. Characterization of the synthesized samples included XRD, XPS, UV-DRS, and scanning electron microscopy. Dopant ions were discovered to coexist with Fe3+ and Fe2+ ions, and to have replaced part of the zinc ions in the crystal lattice. Rhodamine B degradation in aqueous solutions was used to evaluate the photocatalytic activity of the catalysts in both UV and visible light. Photocatalytic activity was found to be greatest in all Fe/ZnO samples when exposed to visible light rather than UV light..

Li et al. [4] reduced graphene oxide (RGO) nanocomposites (ZnO-RGO) were created by reacting zinc chloride (ZnCl2) with graphene oxide (GO) in a single hydrothermal process. Rhodamine B (RhB) was used to measure the photocatalytic activity of the synthetic samples when exposed to artificial sun radiation. The RGO sheets were covered in a homogeneous layer of ZnO nanorods, each having an average diameter of 150 nm. The incorporation of RGO into ZnO nanorods increased light absorption, lowered ZnO size, enhanced the degree of crysatllinity, and stopped ZnO particles from self-aggregating. The nanocomposites had greater photocatalytic effectiveness for RhB degradation than ZnO.

Lam et al. [5] WO3/ZnO nanorods were successfully produced using hydrothermal-deposition, it was reported. They looked examined 2,4-dichlorophenoxyacetic acid (2,4-D)'s photocatalytic breakdown in sunlight. The photocatalytic activity of WO3/ZnO nanorods for 2, 4-D degradation in sunshine was very high. The chemical intermediates and breakdown routes of 2, 4-D were investigated using an HPLC technique, and the appropriate WO3 loading and calcination temperature were determined. Total organic carbon (TOC) and ion chromatography (IC) studies were also performed to evaluate the level of mineralization that occurred during the 2, 4-D degradation.

Saravanan et al. [6] produced a ternary ZnO/Ag/CdO nanocomposite. Spectroscopic, microscopical, and X-ray methods were used to learn more about the nanocomposite. In comparison to binary ZnO/Ag and ZnO/CdO nanocomposites, the ZnO/Ag/CdO nanocomposite showed higher photocatalytic activity under visible light irradiation for the destruction of methyl orange and methylene blue. Under visible light irradiation, the ZnO/Ag/CdO nanocomposite decomposed more than 90% of the industrial textile effluent (actual sample analysis) in 210 minutes.

Bhukal et al. [7] examined the structural, magnetic, electrical, and catalytic characteristics of cobalt zinc ferrites (Co0.6Zn0.4MnxFe2-xO4 (0.2, 0.4, 0.6, 0.8, and 1.0) when Fe3+ ions were replaced by Mn3+ ions. It was discovered that when the concentration of Mn3+ ions increased, the saturation magnetization decreased. It was discovered that, due to the semiconductor nature of nanoferrites, the drift mobility of all compositions decreased with increasing temperature. All of the nanoferrites were tested for their photo-catalytic activity by breaking down methyl orange dye, and it was found that when the quantity of Mn3+ ions was raised from 0.2 to 1.0, the nanoparticles' ability to break down the dye improved. This might be because manganese ions have a larger redox potential and a stronger predilection for octahedral sites than iron ions do.

METHODOLOGY

The chemicals and reagents utilized in this research were all of the highest purity and analytical grade. The whole process relied on double-distilled water, which was produced in an all-glass apparatus (of Borosil brand). P-Nitrophenol was obtained from SISCO Chem, Rose Bengal (RB) was purchased from Merck chemical, Malachite Green (MG) was purchased from Loba Chemie, and Celestin Blue (CB) was purchased from Merck chemistry, India. The degradation experiment used them in this form.

PHOTOCATALYST CHARACTERIZATION

The following techniques were used to characterize the produced nanocomposites. BaSO4 was used as the standard for recording UV-Vis-DRS on a UV-2450 spectrophotometer (Shimadzu Corporation, Japan). Using the industry-standard KBr pellet method, we were able to describe the surface structure using an FT-IR spectrometer (JASCO-FT-IR-460 Plus). The crystallite size was calculated from the XRD pattern acquired on an X- ray diffractometer (XPERT PRO) using Cu K radiation at 25°C. We used a JSM 6701F-6701 scanning electron microscope (SEM) to take images in secondary and backscattered electron modes. Energy dispersive X-ray spectroscopy (EDX) coupled to the SEM detected the elemental analyses. Transmission electron microscopy (TEM) using a TECNAI G2 model was also used to examine the surface morphology.Average pore diameters were calculated

from the N2 adsorption-desorption isotherm using the Barrett-Joyner-Halenda (BJH) method, and the B.E.T surface area was evaluated using a volumetric adsorption analyzer (MICROMERITICS, ASAP 2020). At room temperature, a xenon lamp was used as the excitation light source for the fluorescence spectrophotometer (JASCO- FP-6500) that was used to detect the photoluminescence (PL) spectra. Spectra of adsorption were collected using a UV-visible spectrophotometer (JASCO-V-530). A pH meter (EUTECH) was used to check the pH level. The HEBER immersion photoreactor (HIPR-MP125) was used for the photodegradation studies. [10]

Diffuse reflectance UV-Visible spectroscopic studies (DRS)

When it comes to the optical characterisation of powder or crystalline materials, diffuse reflectance is a fantastic sampling method. Diffuse reflectance requires the spectrometer beam to be projected precisely into the sample, where it will be scattered, reflected, and ultimately transmitted. The accessory collects the back-reflected, diffusely dispersed light (part of which is absorbed by the sample) and guides it toward the detector optics. Diffuse reflection only applies to the fraction of the beam that is internally dispersed inside a sample and reflected back to the surface. In the range of 200 to 600 nm, using barium sulfate (BaSO4) as a standard, UV-vis diffuse reflectance spectra (DRS) of the produced powder samples were recorded using a Shimadzu UV2550 UV-vis spectrophotometer fitted with an integrating sphere attachment (IRS 2200). The sample is gently stuffed into a sample container that has a five square centimeter circular opening..

DATA ANALYSIS

DEGRADATION OF EOSIN YELLOW BY ZN 2SNO4-V2O5 NANOCOMPOSITE PREPARE AND PHOTOCATALYTIC ACTIVITY UNDER VISIBLE LIGHT IRRADIATION

Characterization

- **UV- vis DRS**

Figure displayed the UV-Vis diffuse reflectance spectra of the as-prepared samples. When compared to pure Zn2SnO4 and V2O5, the absorption edges of 2%, 3%, and 5% Zn2SnO4-V2O5 nanocomposites are around 345 and 550 nm, respectively, indicating a slight red shift. Zn2SnO4-V2O5's red shift is due to the electron-hole transition between the two materials. As the semiconductor's absorption edge gets farther out into the visible spectrum, the band gap tends to get smaller. Bandgap values are shown in Fig. for Zn2SnO4,V2O5, 2% Zn2SnO4 -V2O5, 3% Zn2SnO4 - V2O5, and 5% Zn2SnO4 - V2O5, respectively, ranging from 3.6eV to 1.98eV.Since ZnSnO4, V2O5 absorbs less visible light than Zn2SnO4, a 3% mixture of the two absorbs more light.

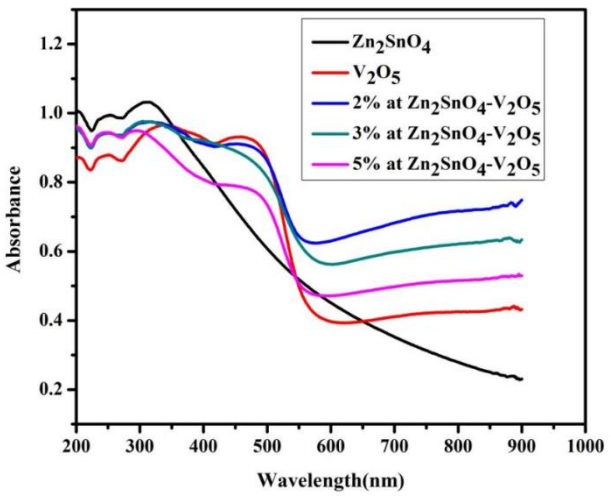

Figure 1: UV-Vis-DRS of Zn_2SnO_4, V_2O_5, 2% Zn_2SnO_4 - V_2O_5, 3% Zn_2SnO_4 - V_2O_5 and 5%Zn_2SnO_4-V_2O_5

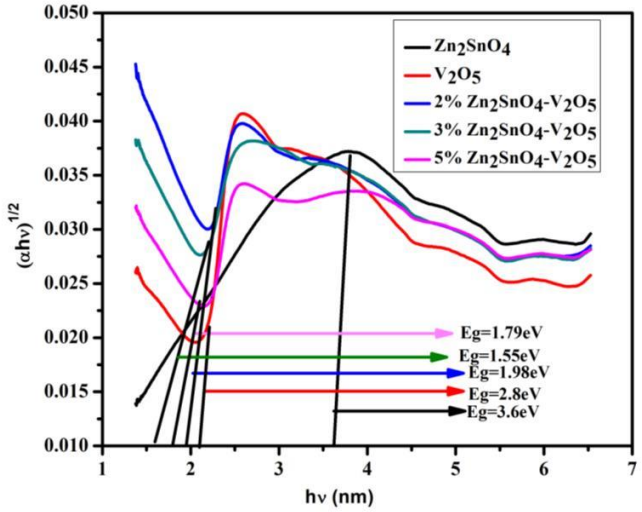

Figure 2: $(\alpha E_{photon})^{1/2}$ Vs E_{photon} curve of Zn_2SnO_4, V_2O_5, 2% Zn_2SnO_4 - V_2O_5, 3% Zn_2SnO_4 - V_2O_5 and 5% Zn_2SnO_4 - V_2O_5

According to this empirical expression, the calculated CB (E_{CB}) and VB (E_{VB}) edge position for Zn_2SnO_4 and V_2O_5 are listed in Table .

Table 1: Estimated band-gap energies (E_g) and calculated E_{VB} and $E_{CB}$of Zn_2SnO_4, V_2O_5

Catalyst	X(eV)	E_{VB} (eV)	E_{CB} (eV)	E_g (eV)
Zn_2SnO_4	10.48	7.78	4.18	3.6
V_2O_5	7.87	4.77	1.97	2.8

FT-IR Spectrum

The FT-IR spectra of Zn_2SnO_4, V_2O_5 and Zn_2SnO_4 - V_2O_5 nanocomposite are shown in Fig.. The main characteristic peaks of Zn_2SnO_4 and V_2O_5 are in accordance with the reported results respectively. We can see that the three samples exhibit similar characteristics of infrared adsorption bands, which are quite similar to the Zn_2SnO_4 reported in previous literature . Therein, the broad absorption peaks at 3426 and 1602 cm^{-1} can be ascribed to the vibration of absorptive water, and the absorption peaks at ,546, 1038, and 1410 cm^{-1} are due to the vibration of M–O or M–O–M groups in Zn_2SnO_4 . Two characteristic absorption bands at 824 cm^{-1} and 1014 cm^{-1} are observed in V_2O_5 sample. The band at 824 cm^{-1} is assigned to the asymmetric stretching modes of V- O-V bond and other peak at 1014 cm^{-1} is attributed to the stretching vibration of V=O bond. Further, the FT-IR spectra of Zn_2SnO_4 - V_2O_5 composites represent the overlap of the Zn_2SnO_4 - V_2O_5 spectra. The FT-IR peak intensity of V_2O_5 is decreased with increase in the mole percent of Zn_2SnO_4. This indicates the coexistence of the Zn_2SnO_4 and V_2O_5in the composite.

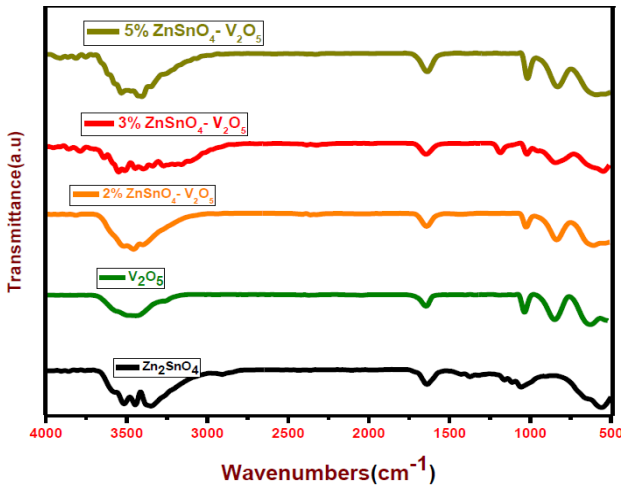

Figure 3: FT-IR spectrum of Zn_2SnO_4, V_2O_5, 2% Zn_2SnO_4-V_2O_5 3% Zn_2SnO_4-V_2O_5 and 5% Zn_2SnO_4-V_2O_5

X-ray diffraction

The crystal structure identity and phase composition of pure Zn_2SnO_4, V_2O_5, Zn_2SnO_4 -V_2O_5 nanocomposite have been confirmed by XRD patterns and are displayed in Fig.4.4. The X-ray diffraction of Zn_2SnO_4 -V_2O_5 nanocomposite with varying Zn_2SnO_4 contents along with pure Zn_2SnO_4 and V_2O_5 for comparison details also investigated. The pure Zn_2SnO_4 sample possesses dominant diffraction peaks at 2θ with an angle of 17.7°, 23.1°, 29.1°, 34.3°, 41.7°, 51.7°, 55.1° and 60.4° representing the indices of (1 1 1), (0 1 2), (2 2), (3 1 1), (4 0 0), (4 2 2), (5 1 1) and (4 4 0) lattice planes in the cubic phase Zn_2SnO_4 (JCPDS no: #74-2184 card), respectively. As for the pure V_2O_5 sample, it can be noted that the main diffraction peaks detected, i.e 15.3°, 20.2°, 25.4°, 26.0°, 32.3°, 34.2°, 40.0°, 49.3° and 55.5°can be assigned to the (2 0 0), (0 0 1), (2 0 1), (1 1 0), (0 1 1), (3 1 0), (3 1 1), (1 1 2) and (0 2 1) lattice planes in the orthorhombic phase V_2O_5 (JCPDS no: #89-2482 card). High degrees of crystallinity are indicated by the narrowing and well-defined of the diffraction peaks of Zn2SnO4 and V2O5. Diffraction patterns of Zn2SnO4 and V2O5 samples showed no impurity-related peaks, proving their great purity. Diffraction patterns reveal that the Zn2SnO4-V2O5 nanocomposite is composed of just two phases: the orthorhombic phase of V2O5 and the cubic phase of Zn2SnO4. Since only Zn2SnO4 and V2O5 existed, the nanocomposites were denoted as such.

$$D = k\lambda / \beta\cos\theta \quad \text{----------} \quad (1)$$

Where D is the average crystallite size, β is the full width half maximum (FWHM) of the highest intensity peak (110 peak), k is a shape of factor of the particles (it equals to 0.89). The average crystalline sizes of Zn_2SnO_4, V_2O_5, 2% Zn_2SnO_4 - V_2O_5, 3% Zn_2SnO_4 - V_2O_5, 5% Zn_2SnO_4 - Scherrer equation was used to determine the atomic radii of V2O5 nanocomposite, and the resulting radii are 23.45, 24.53, 26.72, 28.45, and 30.56. The nanocomposite will be stabilized by halting the crystallization process because to the strong contact between the cubic phase of Zn2SnO4 and the orthorhombic phase of V2O5.

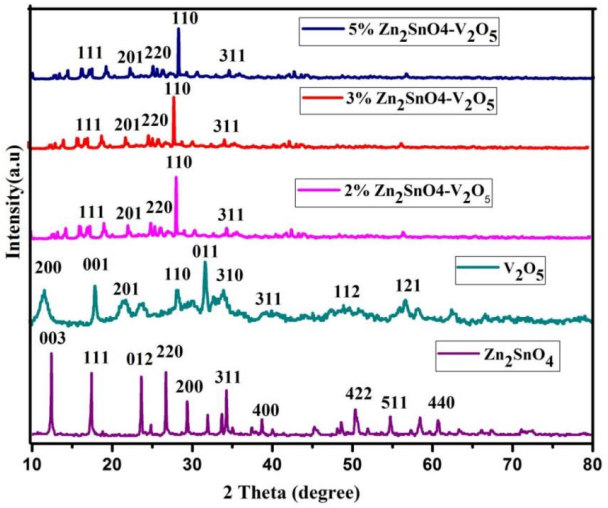

Figure 4: XRD Pattern of Zn_2SnO_4, V_2O_5, 2%Zn_2SnO_4-V_2O_5 3% Zn_2SnO_4–V_2O_5 and 5% Zn_2SnO_4-V_2O_5

Morphological studies

SEM and EDAX were used to examine the microstructure and morphology of pure Zn2SnO4, V2O5, and 3% Zn2SnO4-V2O5. The morphology of pure Zn2SnO4 is shown in Fig. (a-c) to be ball-shaped aggregates, whereas that of V2O5 is shown to be aggregates of various shapes. The morphology of the 3% Zn2SnO4-V2O5 mixture, however, seems to be uniformly spherical, and the average particle size is below 26 nm. As can be seen in Fig. (d), the EDAX analysis of Zn2SnO4-V2O5 composites reveals the presence of components such as Zn, Sn, V, and O.

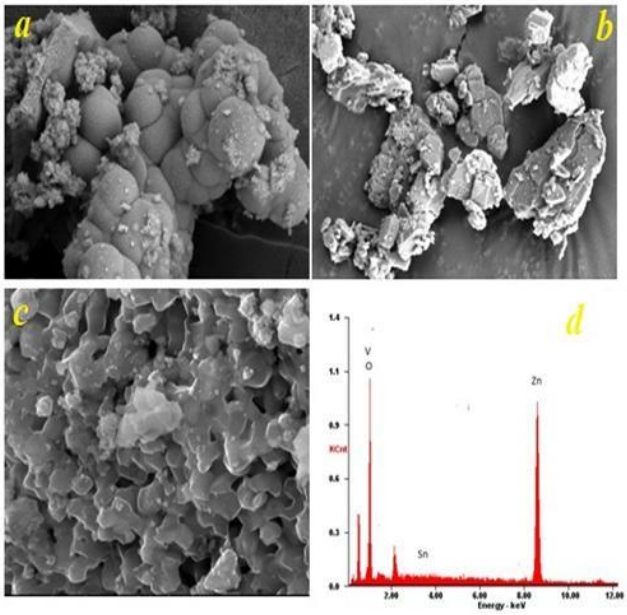

Figure 5: SEM image of (a) Zn_2SnO_4 (b) V_2O_5 (c) 3% Zn_2SnO_4-V_2O_5 (d) EDAX image of 3% Zn_2SnO_4 - V_2O_5

The TEM analysis was carried out to learn more about the photocatalyst's crystalline structure. Nanocomposite of ZnSnO4 and V2O5 at a 3 percent ratio is displayed in TEM (Fig. a). The typical spherical diameter of Zn2SnO4-V2O5 is between 23 and 47 nm, as seen in the picture. The TEM micrograph reveals that V2O5 nanoparticles have been deposited on the Zn2SnO4 plates, producing a darker picture than that of pure Zn2SnO4 plates. Multiple physical and chemical changes occurred in the as-prepared composite during calcination at 80 °C. Mesoporous structures arise when water, including adsorbed, intercalated, and hydroxyl water, is removed from the structure. In Fig.(b), we see the chosen region electron diffraction pattern for the 3% Zn2SnO4-V2O5 nanocomposite. The cubic phase of Zn2SnO4 and the orthorhombic phase of V2O5 are clearly visible in the SAED pattern of the Zn2SnO4-V2O5 nanocomposite, which is in excellent agreement with the XRD pattern. Light patches correspond to the (1 1 1), (2 2 0), (3 1 1), and (4 4 0) planes of the cubic phase of 3% Zn2SnO4-V2O5, while the brighter inner ring corresponds to the orthorhombic phase of V2O5. The spots verify that the 3% Zn2SnO4-V2O5 is a single crystal. As seen by the SAED pattern, the 3% Zn2SnO4-V2O5 nanocomposite has successfully crystallized.

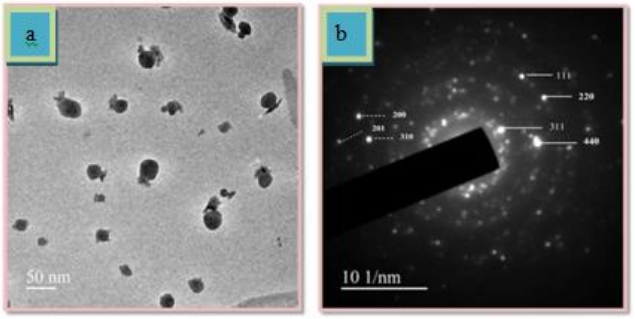

Figure 6: TEM image of (a) 3% Zn_2SnO_4 - V_2O_5 (b) SAED pattern of 3% Zn_2SnO_4 - V_2O_5

BET surface area analysis

The surface of photocatalysts is often where the reaction occurs. The difference in subsequent photocatalytic performance can be understood by examining the isotherms depicted in Fig., which show the specific surface area and pore structure of as-prepared Zn2SnO4,V2O5, and 3% Zn2SnO4-V2O5nanocomposite at -195.609oC through the use of nitrogen adsorption-desorption. All three isotherms may be classified as type IV thanks to their mesoporous character, as defined by the International Union of Pure and Applied Chemistry. Type H3 hysteresis loops describe the hysteresis patterns.The relative pressure hysteresis loop P/P0 is between 0.6 and 1. The average pore size, pore volume, and BET surface area of as-synthesized samples are summarized in a table.

Table 2: Calculated values from N2 adsorption-desorption experiments

Sample	Specific surface area (m^2/g)	Average pore diameter (nm)	Pore volume (cm^3/g)
Zn_2SnO_4	40.76	33.38	0.4359
V_2O_5	38.45	44.41	0.4509
3% Zn_2SnO_4- V_2O_5	57.65	88.66	1.2234

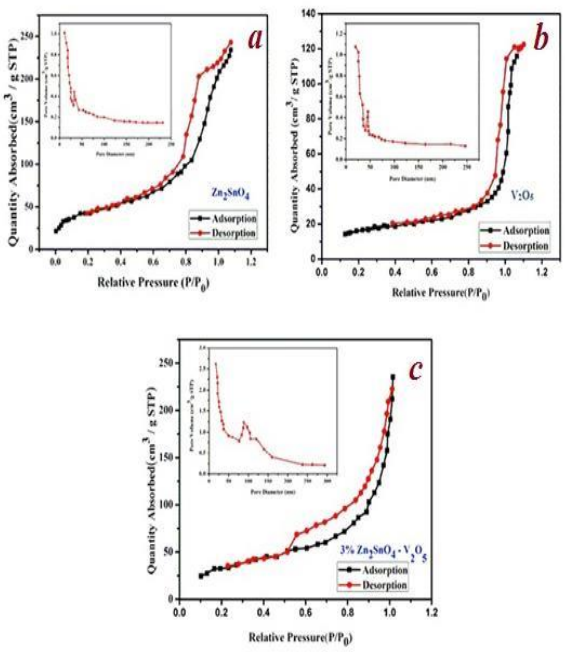

Figure 7: N_2 adsorption – desorption isotherms and pore size istribution plots for sample of (a) Zn_2SnO_4 (b)V_2O_5 (c) 3% Zn_2SnO_4 - $_2O_5$

Photocatalytic degradation of EY

Maximum absorption in the UV-Vis range was measured over time to observe photocatalytic degradation. At a concentration of 3% the photocatalytic activity of a Zn2SnO4 -V2O5 nanocomposite was evaluated by monitoring its ability to degrade EY at pH4. It was discovered that the concentration of EY under visible light irradiation scarcely photodegraded in the absence of the photocatalytic components. Dark experiments with photocatalytic materials for 30 minutes revealed that the active sites of the synthesized photocatalysts absorbed more dye the longer they were exposed to light. The eV absorption peak at max 595 nm gradually decreased after being exposed to light for 180 minutes. The photocatalytic degradation of EY in aqueous solution with 3% Zn2SnO4 -V2O5 was 92% effective. Because no other absorption bands could be found in the visible or ultraviolet spectrum, it was assumed that the conjugated structure had been broken down.

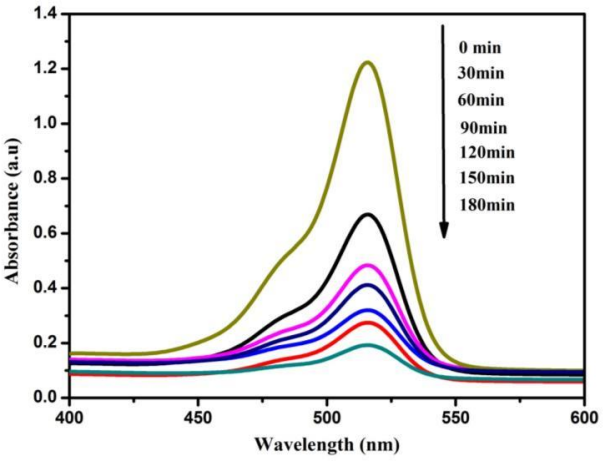

.

Figure 8: Time Dependent UV-Vis spectral changes of EY (1.5µM) in Presence of (3% Zn_2SnO_4 -V_2O_5) (0.375g/L)

Using the literature on the photocatalyltic activity of nanocomposites, we propose a mechanism for the enhanced photocataltic activity of 3% Zn2SnO4-V2O5. Irradiation-induced electron transport is shown in a simplified schematic form in Fig. with visible light via 3% Zn2SnO4-V2O5. This is because when 3% Zn2SnO4-V2O5 is exposed to visible light, more electrons and holes are formed in the conduction band and valence band of Zn2SnO4 due to its small band gap. Zn2SnO4's photo-generated electrons readily enter the conduction band of V2O5, whereas V2O5-Zn2SnO4 holes go in the other way. As a result, effective electron - holes separation is obtained on the nanocomposites' surface, and the electron - holes recombination process is greatly reduced. Capturing electrons from the conduction band allows photodegradation of EY, while holes oxidize H2 to produce water.

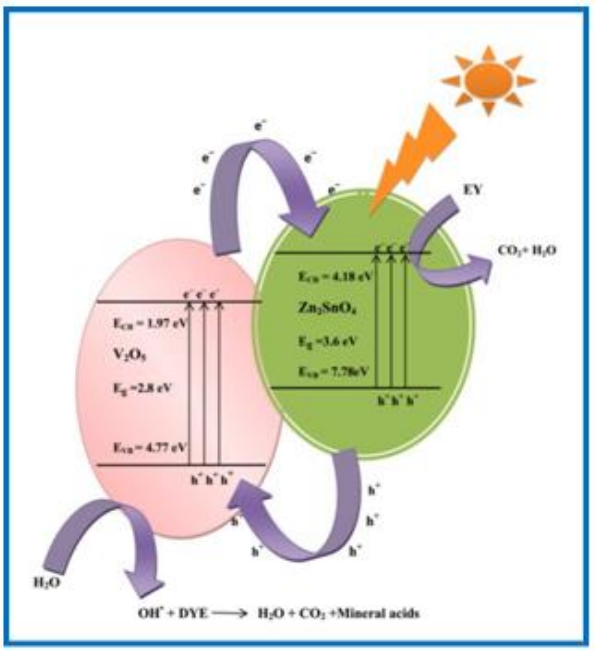

Figure 4.9: The schematic diagram of electron

transfers in 3% Zn_2SnO_4 - V_2O_5 under visible-light irradiation.

CONCLUSION

It can be concluded that the synthesis and characterisation of TiO2/GO nanocomposites for photocatalytic degradation of organic pollutants under visible light irradiation is a viable technique for the development of effective and environmentally friendly photocatalysts. This research shows how nanocomposites may be used to improve the photocatalytic activity of materials and offers guidance for designing and optimizing photocatalytic materials. In conclusion, photocatalytic degradation of organic pollutants using nanocomposites under visible light has significant potential for environmental remediation. However, more study is required to improve their qualities and uncover their working mechanisms. This study synthesizes and efficiently employs five distinct heterogeneous nanocomposites as a visible light driven photocatalyst for the elimination of contaminants. The following is a summary of the findings concerning the photocatalytic activity of five distinct catalysts. High adsorption-photocatalysis was achieved by the use of a NiO/Ag3VO4 hybrid in this research. UV-DRS, FT-IR, XRD, SEM, TEM, SAED, EIS, and BET-surface analysis all gave accurate descriptions of the synthesized photocatalyst. Visible light irradiation resulted in rapid photodegradation of 4-NP and RB in the NiO/Ag3VO4 composite. The visible light absorption of the NiO/Ag3VO4 composite was enhanced, and the UV-vis absorption spectra showed that the absorption edge of the composite had moved to a redder color.

REFERENCE

1. X. Zhou, T. Shi and H. Zhou, Hydrothermal preparation of ZnO-reduced graphene oxide hybrid with high performance in photocatalytic degradation, Applied Surface Science, 258 (2012) 6204– 6211.
2. R. Huo, Y. Kuang, Z Zhao, F. Zhang and S. Xu, Enhanced photocatalytic performances of hierarchical ZnO/ZnAl2O4 microsphere derived from layered double hydroxide precursor spraydried microsphere, Journal of Colloid and Interface Science, 407 (2013)17–21.
3. S. Yi, J. Cui, S. Li, L. Zhang, D. Wang and Y. Lin, Enhanced visible-light photocatalytic activity of Fe/ZnO for Rhodamine B degradation and its photogenerated charge transfer properties, Applied Surface Science, 319 (2014) 230–236.
4. X. Li, Q. Wang, Y. Zhao, W. Wu, J. Chen and H. Meng, Green synthesis and photo-catalytic performances for ZnO-reduced graphene oxide nanocomposites, Journal of Colloid and Interface Science, 411 (2013) 69–75.
5. S.-M. Lam, J.-C. Sin, A. Z. Abdullah and A. R. Mohamed, Sunlight responsive WO3/ZnO nanorods for photocatalytic degradation and mineralization of chlorinated phenoxyacetic acid herbicides in water, Journal of Colloid and Interface Science, 450 (2015) 34–44.
6. R. Saravanan, M. M. Khan, V. K. Gupta, E. Mosquera, F. Gracia, V. Narayanan and A. Stephen, ZnO/Ag/CdO nanocomposite for visible light-induced photocatalytic degradation of industrial textile effluents, Journal of Colloid and Interface Science, 452 (2015) 126–133.
7. S. Bhukal, S.Bansal and S. Singhal, Magnetic Mn substituted cobalt zinc ferrite systems: Structural, electrical and magnetic properties and their role in photo-catalytic degradation of methyl orange azo dye, Physica B, 445 (2014) 48–55.
8. N. Salah, A. Hameed, M. Aslam, S. S. Babkair and F.S. Bahabri, Photocatalytic activity of V doped ZnO nanoparticles thin films for the removal of 2- chlorophenol from the aquatic environment under natural sunlight exposure, Journal of Environmental Management, 177 (2016) 53-64.
9. O. Bechambi, M. Chalbi, W. Najjar and S. Sayadi, Photocatalytic activity of ZnO doped with Ag on the degradation of endocrine disrupting under UV irradiation and the investigation of its antibacterial activity, Applied Surface Science, 347 (2015) 414–420.
10. N. Song, H. Fan and H. Tian, Reduced graphene oxide/ZnO nanohybrids: Metallic Zn powder induced one-step synthesis for enhanced photocurrent and photocatalytic response, Applied Surface Science, 353 (2015) 580–587.
11. C. Dong, X. Xiao, G. Chen, H. Guan and Y. Wang, Synthesis and photocatalytic degradation of methylene blue over p-n junction Co3O4/ZnO core/shell nanorods, Materials Chemistry and Physics, 155 (2015) 1-8.
12. Y.-Y. Bu, Enhanced photocatalytic activity of sol–gel derived ZnO via the co-doping process, Superlattices and Microstructures, 86 (2015) 36–42.

Corresponding Author

Km. Manisha Verma*

PhD Student, Kalinga University Raipur CG